Chaoticity and shell effects in the nearest-neighbor distributions for an axially-symmetric potential

J. P. Blocki[1] and A. G. Magner[2,*]
[1]*National Center for Nuclear Research, Otwock 05-400, Poland*
[2]*Institute for Nuclear Research of the National Academy of Sciences of Ukraine, Kiev 03680, Ukraine*
(Received 28 March 2012; published 11 June 2012)

Statistics of the single-particle levels in a deformed axially symmetric Woods-Saxon potential is analyzed in terms of the Poisson and Wigner nearest-neighbor spacing distributions for several deformations and multipolarities of the surface distortions. We found the significant differences of all the distributions with a fixed value of the angular momentum projection of the particle on the symmetry axis, more closely to the Wigner distribution, in contrast to the full spectra with Poisson-like behavior. The shell effects in the nearest-neighbor spacing distributions, for both small and large deformations of the surface are analyzed.

DOI: 10.1103/PhysRevC.85.064311 PACS number(s): 21.60.Cs, 21.10.Pc, 24.60.Lz, 02.50.−r

I. INTRODUCTION

The microscopic many-body interaction of particles of Fermi systems such as heavy nuclei is rather complicated. Therefore, several theoretical approaches to the description of the Hamiltonian which are based on the statistical properties of its discrete levels are applied for solutions of realistic problems. For a quantitative measure of the degree of chaoticity of the many-body forces, the statistical distributions of the spacing between the nearest-neighboring levels were introduced in relation to the so-called random matrix theory [1–5]. Integrability (order) of the system was associated usually to the Poisson-like exponentially decreasing dependence on the spacing variable with a maximum at zero while chaoticity was connected more to the Wigner-like behavior with the zero spacing probability at zero and a maximum at some finite value of this variable.

On the other hand, many dynamical problems, in particular, in nuclear physics can be reduced to the collective motion of independent particles in a mean field with a relatively sharp time-dependent edge usually called the effective surface within the microscopic-macroscopic approximation [6,7]. We may begin with the basic ideas of Swiatecki and his collaborators [6,8–13]. In recent years it became apparent that the collective nuclear dynamics is very much related to the nature of the nucleonic motion. This behavior of the nucleonic dynamics is important in physical processes like fission or heavy ion collisions where a great amount of the collective energy is dissipated into chaotic nucleonic motion. We have to mention here also very intensive studies of the one-body dissipative phenomena described largely through the macroscopic wall formula for the excitation energy [8–13] and also quantum results [9,11,13,14]. The analytical wall formula was suggested originally in Ref. [8] on the basis of the Thomas-Fermi approach. It was rederived in many works based on semiclassical and quantum arguments (see Refs. [15–17], for instance). However, some problems in the analytical study of a multipolarity dependence of the smooth one-body friction and its oscillating corrections as functions of the particle number should still be clarified. In particular, we would like to emphasize the importance of the transparent classical picture through the Poincaré sections and Lyapunov exponents showing the order-chaos transitions [10,18–20] and also quantum results for the excitation energy [11,13,14]. Then, the peculiarities of the excitation energies for many periods of the oscillations of the classical dynamics were discussed for several Legendre polynomials (see Ref. [14]) as the classical measures of chaoticity. The shell-correction method [7,21] was successfully used to describe the shell effects in the nuclear deformation energies as functions of the particle numbers. This is important also for understanding analytically the origin of the isomers in fission within the periodic orbit theory (POT) [22]. We should expect also that the deviations of the level density near the Fermi surface, like shell effects, from an averaged constant should influence essentially the nearest-neighbor spacing distribution (NNSD). For further study of the order-chaos properties of the Fermi systems, it might be worth applying the statistical methods of the description of the single-particle (SP) levels of a mean-field Hamiltonian within microscopic-macroscopic approaches (see, for instance, Refs. [23–26]).

The relation of the statistics of the spacing between the neighboring levels and the shell effects depending on the specific properties of the SP spectra, as well as the multipolarity and deformation of the shape surfaces should be expected. The quantitative measure of the order (or symmetry) can be the number of the single-valued integrals of motion $\mathcal{K}$, besides the energy (degree of the degeneracy of the classical and quantum systems, see also Refs. [22,27–29]). If the energy is the only one single-valued integral of motion ($\mathcal{K} = 0$) one has the completely chaotic system [30]. For the case of any additional integral of motion, say the angular momentum projection for the azimuthal symmetry ($\mathcal{K} = 1$), one finds the symmetry enhancement which is important for calculations of the level density as the basic characteristics of the SP spectra.

Our purpose now is to look at the order-chaos properties of the SP levels in terms of the Poisson and Wigner distributions with focus to their dependence on the multipolarities, deformations, and shell effects in relation to the integrability of the Hamiltonian through the comparison between the spectra with

*magner@kinr.kiev.ua

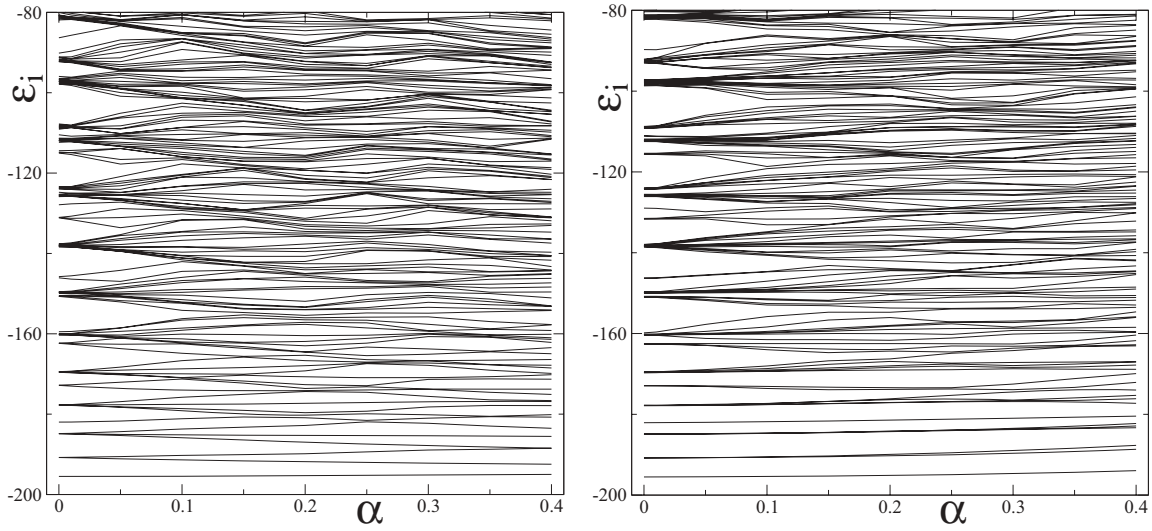

FIG. 1. SP energy levels ε_i in WS potential ($V_0 = 200$ MeV, $R_0 = 6.622$ fm, $a = 0.1$ fm) as a function of the deformation α for the P_2 (left) and P_5 (right) shapes [Eq. (3)].

the fixed angular momenta of particles and the full ones for the axially symmetric Woods-Saxon potential.

II. SPECTRA AND LEVEL DENSITIES

We are going now to study the statistical properties of the SP spectra of the eigenvalue problem

$$H\phi_i = \varepsilon_i \phi_i, \quad H = T + V, \tag{1}$$

where H is a static mean-field Hamiltonian with the operator of the kinetic energy T and deformed axially symmetric Woods-Saxon (WS) potential V:

$$V \equiv V_{\mathrm{WS}}(\mathbf{r}) = -\frac{V_0}{1 + \exp\{[r - R(\theta)]/a\}}, \tag{2}$$

where r, θ, φ are the spherical coordinates of the vector $\mathbf{r}$. Following Refs. [9,10,12,13], the shape of the WS-potential surface is defined by the effective radius $R(\theta)$ given by

$$R(\theta) = \frac{R_0}{\lambda}\left[1 + \alpha\sqrt{\frac{4\pi}{5}}Y_{n0}(\theta) + \alpha_1\sqrt{\frac{4\pi}{3}}Y_{10}(\theta)\right]. \tag{3}$$

Here, λ is a normalization factor ensuring volume conservation, α_1 stands for keeping position of the center of mass at $z = 0$ for odd multipolarities, R_0 is the radius of the equivalent sphere, and $Y_{n0}(\theta) = \sqrt{(2n+1)/(4\pi)}P_n(\cos\theta)$ are the spherical functions. $P_n(\cos\theta)$ are the Legendre polynomials and α is the deformation parameter and is independent of time. In the expansion (3) we consider only single Legendre polynomials just to see how different polynomials influence the picture. For diagonalization of the Hamiltonian with the WS potential (2),

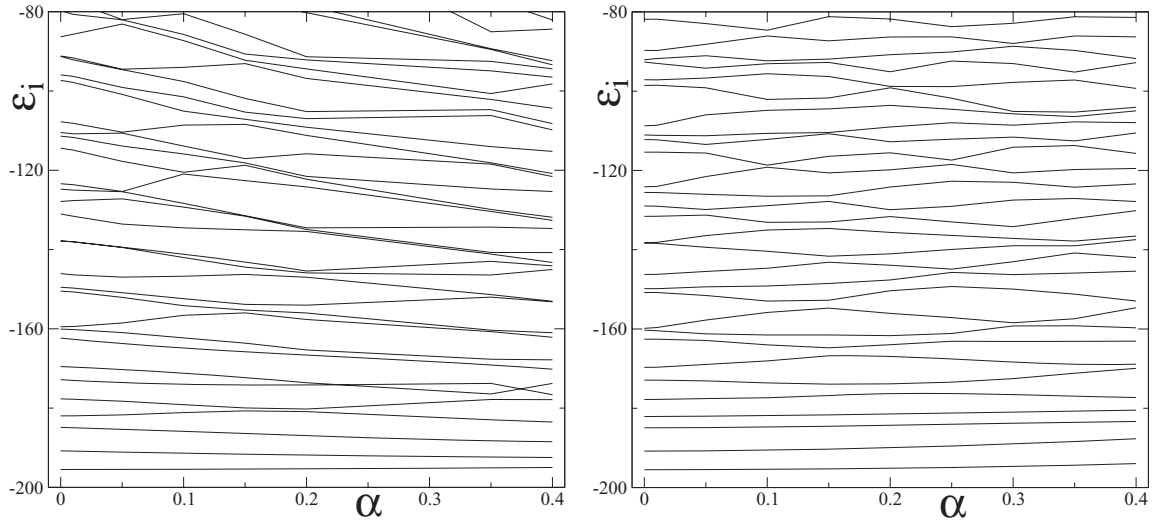

FIG. 2. Same SP spectrum of levels as in Fig. 1 but with projection of angular momentum $m = 0$.

the expansion over a basis of the deformed harmonic oscillator is used as shown in Ref. [13].

Figures 1 and 2 show two examples for the full spectra of the SP energies ε_i and for the fixed angular momentum projection $m = 0$ versus the deformation parameter α for the P_2 and P_5 shapes, respectively. The spectra for P_3 and P_4 are very similar to the P_5 case and therefore, they are not shown. As seen from Fig. 1, there are clear shell effects in the full spectra at small deformations, approximately at $\alpha \lesssim 0.1$ for all multipolarities from the P_2 shape to the P_5 shape. With increasing deformation α, the shell gaps become less pronounced and slowly change in the region $\alpha \approx 0.1$–0.4 for all these multipolarities. Many more differences can be found in comparison of Fig. 1 for full spectra and Fig. 2 for $m = 0$ levels only. The shell effects are seen here, too, but much less pronounced. The spectrum of levels with $m = 0$ becomes much more uniform due to the fixing of m itself, in particular with increasing deformations and multipolarities ($n > 1$).

The key quantity for calculations of the NNSD $P(S)$ is the level density $g(\varepsilon)$. In Appendix where we rederive $P(S)$, according basically to Refs. [1,3,5], with emphasis, however, on the relation of $g(\varepsilon)$ to the SP level density as well as the meaning of its argument ε. For these calculations one may apply the Strutinsky shell correction method, writing

$$g_\Gamma(\varepsilon) = \tilde{g}(\varepsilon) + \delta g_\Gamma(\varepsilon). \tag{4}$$

The smooth part $\tilde{g}(\varepsilon)$ is defined by the Strutinsky smoothing procedure [7,21]. The so-called plateau condition (stability of values of the smooth level density $\tilde{g}$ as function of the averaging parameters: Gaussian width Γ and the degree of the correction polynomial M takes place at $\Gamma = 20$–40 MeV and $M = 4$–8). Note that the smooth level density $\tilde{g}(\varepsilon)$ can be well approximated by the extended Thomas-Fermi model [29]. Figures 3 and 4 for the full spectra and for the fixed angular momentum projection $m = 0$ show typical examples of the level densities (smooth component and total density with oscillating part) for the Legendre polynomials $n = 2$ and 5 at deformations $\alpha = 0.1$ and 0.4, in correspondence with spectra presented in Figs. 1 and 2, respectively. In Fig. 4 for the case of the specific $m = 0$ levels, one has somewhat larger Gaussian-width parameters of the smooth level density $\tilde{g}$ in the total density [Eq. (4)] than those for the full spectra in Fig. 3. As seen clearly from Figs. 3 and 4 the smooth level density for the $m = 0$ spectra is more flat (besides of relatively small remaining oscillations because of much fewer levels with the fixed $m = 0$), as compared with the full-spectrum results. In the semiclassical picture this more flat behavior for the fixed $m = 0$ value is due to the restriction of the phase space for motion of the particle to the two-dimensional (2D) plane going through the symmetry axis. It looks like an extended Thomas-Fermi approximation for three dimensions (3D) and 2D to the corresponding smooth level density.

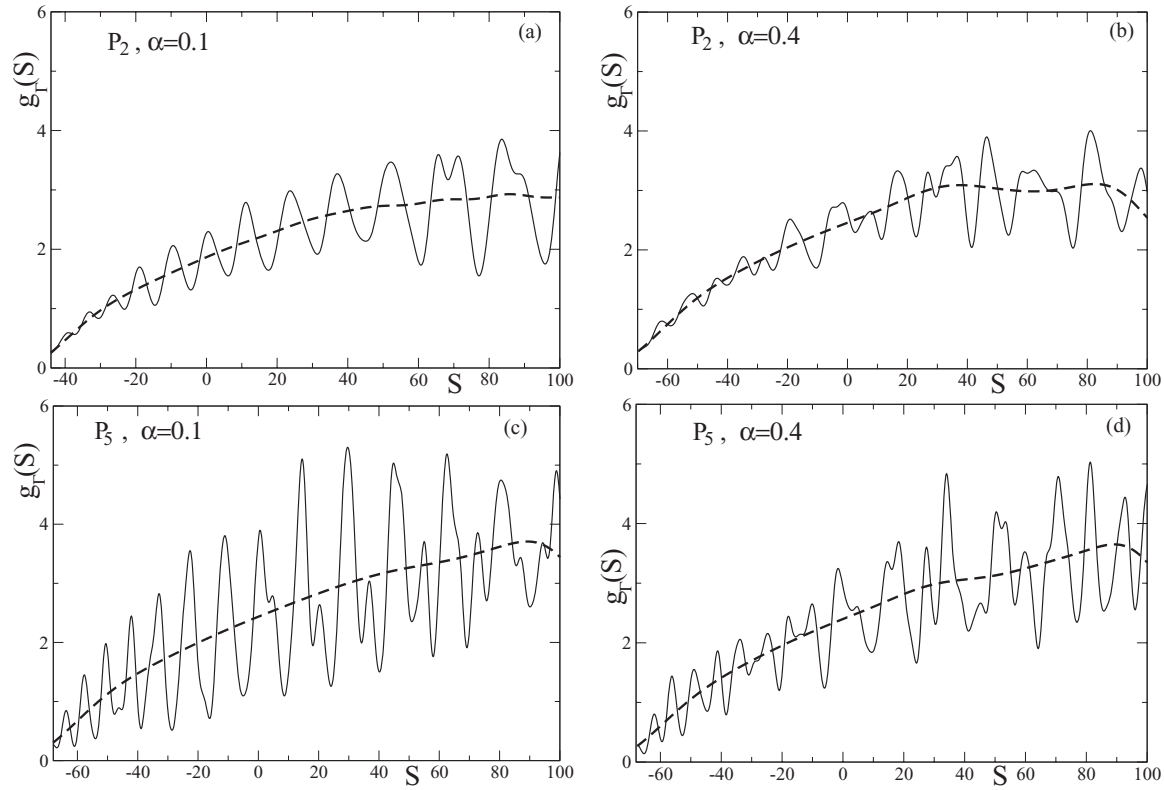

FIG. 3. Level densities $g_\Gamma(S)$ [Eq. (4)] as a function of the energy counted from the Fermi level ($S = 0$) for a given particle number N for spectra of the SP levels of Fig. 1 for the P_2 [(a) and (b)] and P_5 [(c) and (d)] shapes at the small $\alpha = 0.1$ (left panels) and larger $\alpha = 0.4$ (right panels) deformations; dashed line is the smooth density $\tilde{g}(S)$ [Eq. (4)]; solid is the total density $g_\Gamma(S)$ [Eq. (4)] [$\Gamma = 3$ MeV, $M = 0$ for $\delta g_\Gamma(S)$].

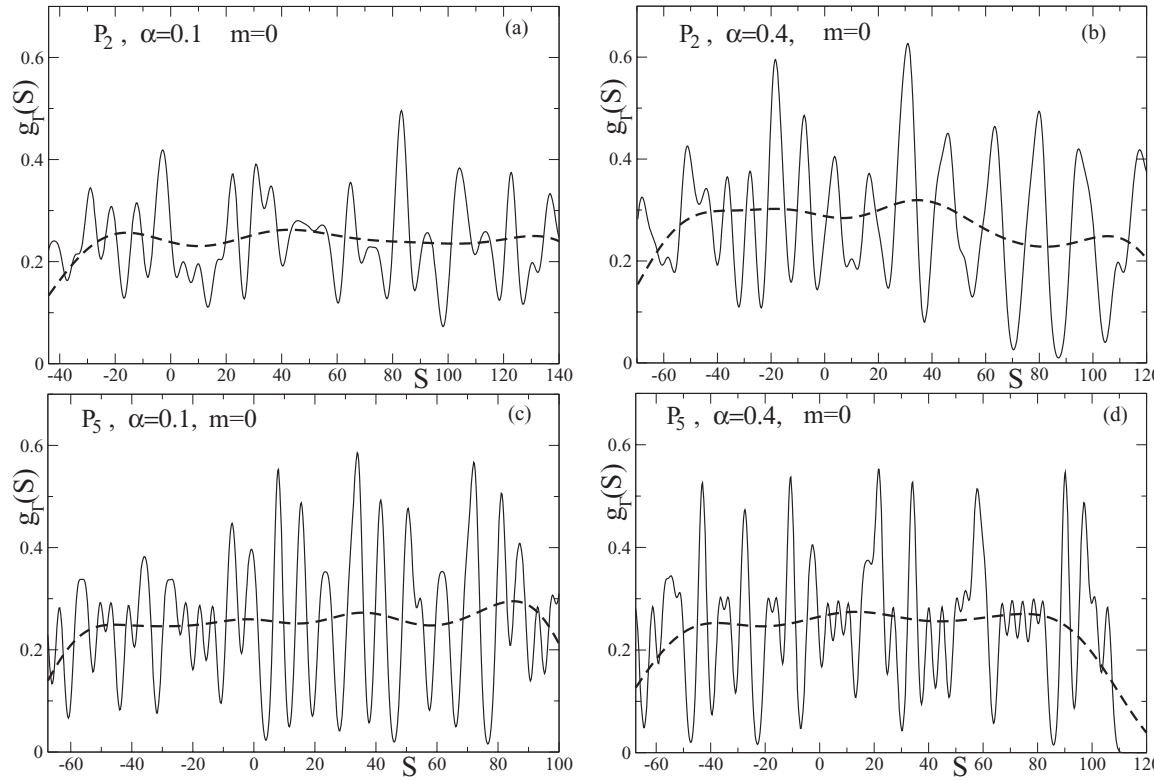

FIG. 4. Same as in Fig. 3 but for levels with fixed projection of angular momentum $m = 0$.

[cf., for example, Eqs. (4.139) and (4.138) in Ref. [29] for billiard systems which are similar to the case of our deep WS potential with sharp edges]. By fixing m, one has the loss of the symmetry degree $\mathcal{K}$ (see introduction) because the 3D motion with the partial integrability ($\mathcal{K} = 1$) caused by the azimuthal symmetry becomes 2D nonintegrable ($\mathcal{K} = 0$) in the phase space restricted to the symmetry-axis plane by the given $m = 0$. Therefore, one expects the system with the fixed angular momentum m to be more chaotic than for full spectra. The differences between Figs. 3 and 4 are quite remarkable. On the other hand, differences between pictures within Figs. 3 or 4 are less notable and as one can see shell effects are still remaining at bigger deformations and multipolarities.

III. NEAREST-NEIGHBOR SPACING DISTRIBUTIONS

Following the review paper [3], the distribution $P(S)$ for the probability of finding the spacing S between the nearest-neighboring levels is given by (see also Refs. [1,2,4,5] and Appendix)

$$P(S) = g(S) \exp\left(- \int_0^S g(x)dx \right) \Big/ \aleph. \tag{5}$$

The key quantity $g(S)$ can be considered as the density of the SP levels counted from a given energy, say, the Fermi energy E_F. D is a mean uniform distance between neighboring levels so that $1/D$ is the mean density of levels. $\aleph$ is the normalization factor for a sufficiently large maximal value of S, $S_{\max}$:

$$\aleph = \int_0^{S_{\max}} dx g(x) \exp\left(- \int_0^x g(y)dy \right) \Big/ D. \tag{6}$$

This normalization factor $\aleph$ can be found from the normalization conditions:

$$\int dx P(x) = \int dx x P(x) = 1. \tag{7}$$

[Notice that, for convenience, we introduced the dimensionless probability P in contrast to that of Ref. [3]; see Eq. (1.3) there.]

The Poisson law follows if we take constant for the level density, $g(S) = 1/D$, in Eq. (5),

$$P(S) = \exp(-S/D). \tag{8}$$

Wigner's law follows from the assumption of the linear level density, proportional to S,

$$P(S) = \left(\frac{\pi S}{2D} \right) \exp\left(-\frac{\pi S^2}{4D^2} \right). \tag{9}$$

Both distributions are normalized to one for sufficiently large maximal value of S, $S_{\max} = \infty$ to satisfy Eq. (7).

The level density in fact is not a constant or $\propto S$. The combinations of the Poisson and Wigner distributions were suggested in Refs. [3,31] by introducing one parameter. For our purpose to keep a link with the properties of the level density, like smooth and shell components [7], it is convenient to define the probability $P(S)$ [Eq. (5)] for a general linear

level-density function through two parameters $\mathcal{A}$ and $\mathcal{B}$:

$$g(S) = (\mathcal{A} + \mathcal{B}S/D)/D. \tag{10}$$

Substituting Eq. (10) into the general formula [Eq. (5)], one obtains explicitly the analytical result in terms of the standard error functions, $\mathrm{erf}(z) = 2\int_0^z dx\, \exp(-x^2)/\sqrt{\pi}$,

$$P(S) = (1 + \mathcal{B}\xi/\mathcal{A})\exp(-\mathcal{B}\xi^2/2 - \mathcal{A}\xi)/[\aleph_0 + \mathcal{B}\aleph_1/\mathcal{A}], \tag{11}$$

$$\begin{aligned}\aleph_0 &= \int_0^{\mathcal{C}} d\xi \exp\left(-\frac{\mathcal{B}}{2}\xi^2 - \mathcal{A}\xi\right) \\ &= \sqrt{\frac{\pi}{2\mathcal{B}}}\exp\left(\frac{\mathcal{A}^2}{2\mathcal{B}^2}\right)\mathrm{erf}\left(\frac{\mathcal{A}+\mathcal{B}\mathcal{C}}{\sqrt{2\mathcal{B}}}\right), \\ \aleph_1 &= \int_0^{\mathcal{C}} d\xi\,\xi \exp\left(-\frac{\mathcal{B}}{2}\xi^2 - \mathcal{A}\xi\right) \\ &= -\frac{1}{\mathcal{B}}\left[\exp\left(-\frac{\mathcal{B}}{2}\mathcal{C}^2 - \mathcal{A}\mathcal{C}\right) + \mathcal{A}\aleph_0\right],\end{aligned} \tag{12}$$

where $\xi = S/D$, $\mathcal{C} = S_{\max}/D$ is the maximal value of ξ. For large $\mathcal{C} \to \infty$ one has simply $\aleph_0 \to \sqrt{\pi/(2\mathcal{B})}\exp[\mathcal{A}^2/(2\mathcal{B}^2)]$ and $\aleph_1 \to -\mathcal{A}\aleph_0/\mathcal{B}$. Taking the limits $\mathcal{A} \to 1$, $\mathcal{B} \to 0$, and $\mathcal{A} \to 0$, $\mathcal{B} \to 1$ in Eq. (11) one simply finds exactly the standard Poisson [Eq. (8)] and Wigner [Eq. (9)] distributions. In this way the constants $\mathcal{A}$ and $\mathcal{B}$ are measures of the probability to have Poisson and Wigner distributions [Eq. (10)]. Note that Eq. (11) for the NNSD $P(S)$ looks similar to Eq. (12) of Ref. [32], except for the sign in front of the second term ($\propto S^2$) of the exponent argument, which is perhaps a misprint. We give also explicitly the analytical normalization function [see Eq. (12)] and more clear relation to the linear level density $g(S)$ (10) through the general NNSD $P(S)$ given by Eq. (5).

IV. NUMERICAL RESULTS

Figures 5 and 6 show the corresponding NNSD $P(S)$ [Eq. (5)]. Again, in accordance with spectra (see Figs. 1 and 2) and level-density calculations in Figs. 3 and 4, dramatic changes are observed between Fig. 6 for the NNSD $P(S)$ with the $m = 0$ and Fig. 5 for those of the full-spectrum ones. Results presented by heavy dots in Fig. 5 look more close to the Poisson distribution and those in Fig. 6 are more close to the Wigner distribution.

There are large differences in numbers $\mathcal{A}$ and $\mathcal{B}$ which measure the closeness of the distributions $P(S)$ for the neighboring levels spacing to the standard ones, Poisson (1,0) and Wigner (0,1). However, in Fig. 6 all distributions are more close to the Wigner distribution in shape, having a maximum between zero and being large with respect to D value $S_{\max} = \mathcal{C}D$ as compared to the monotonic exponential-like decrease similar to the Poisson behavior in Fig. 5. Notice that we have

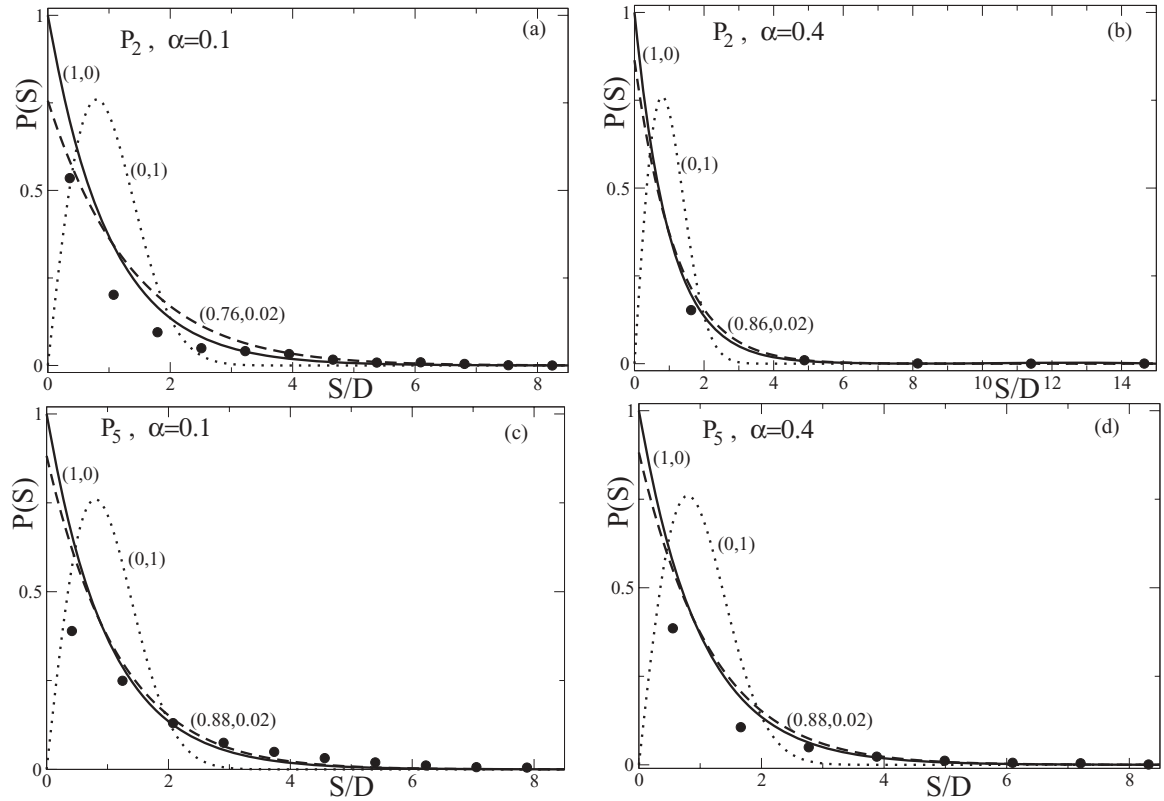

FIG. 5. Distributions of spacing of neighboring levels $P(S)$ represented by heavy dots [3] vs the energies S for the same spectra as in Figs. 1 and 3. Solid curve is a standard Poisson distribution [Eq. (8)] and dotted curve is a standard Wigner distribution [Eq. (9)]. Numbers in brackets ($\mathcal{A}$, $\mathcal{B}$) show $\mathcal{A}$ and $\mathcal{B}$ of Eq. (11). Dashed curve corresponds to a linear approximation to the level density [Eq. (10)]; other notations are the same as in Figs. 3 and 4.

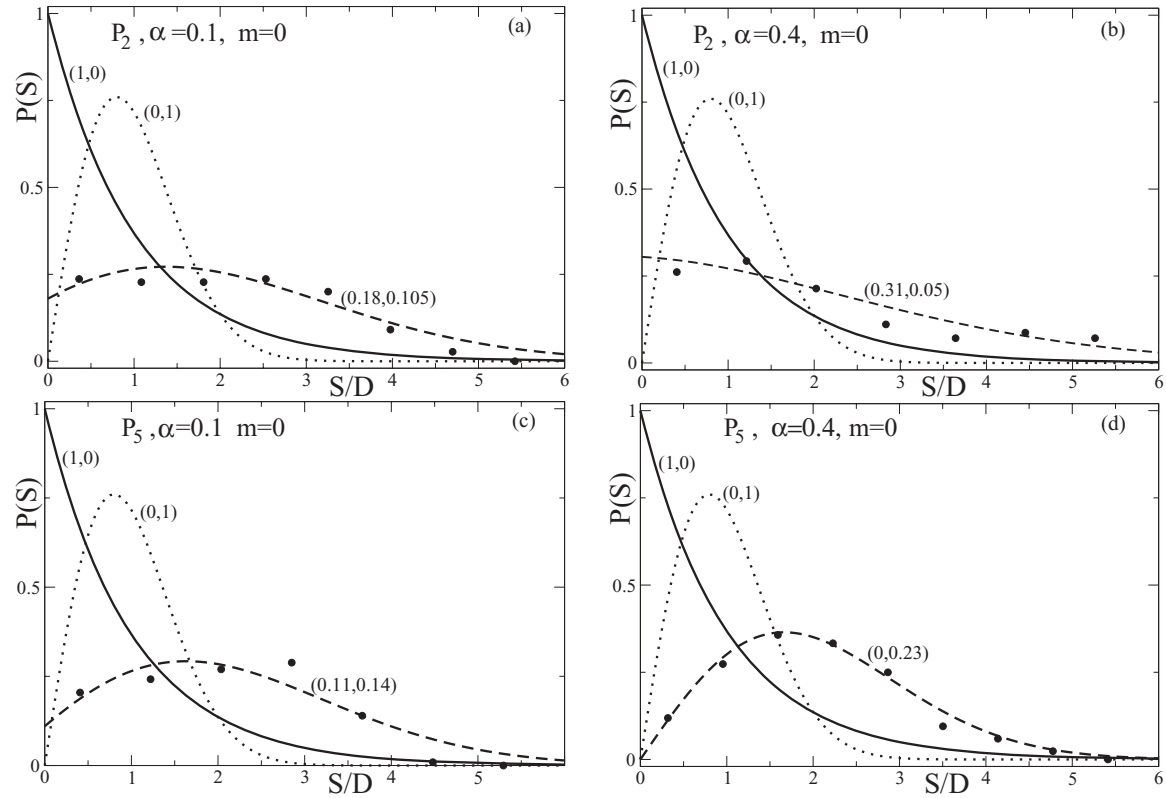

FIG. 6. Same as in Fig. 5 but for the spectra of Figs. 2 and 4.

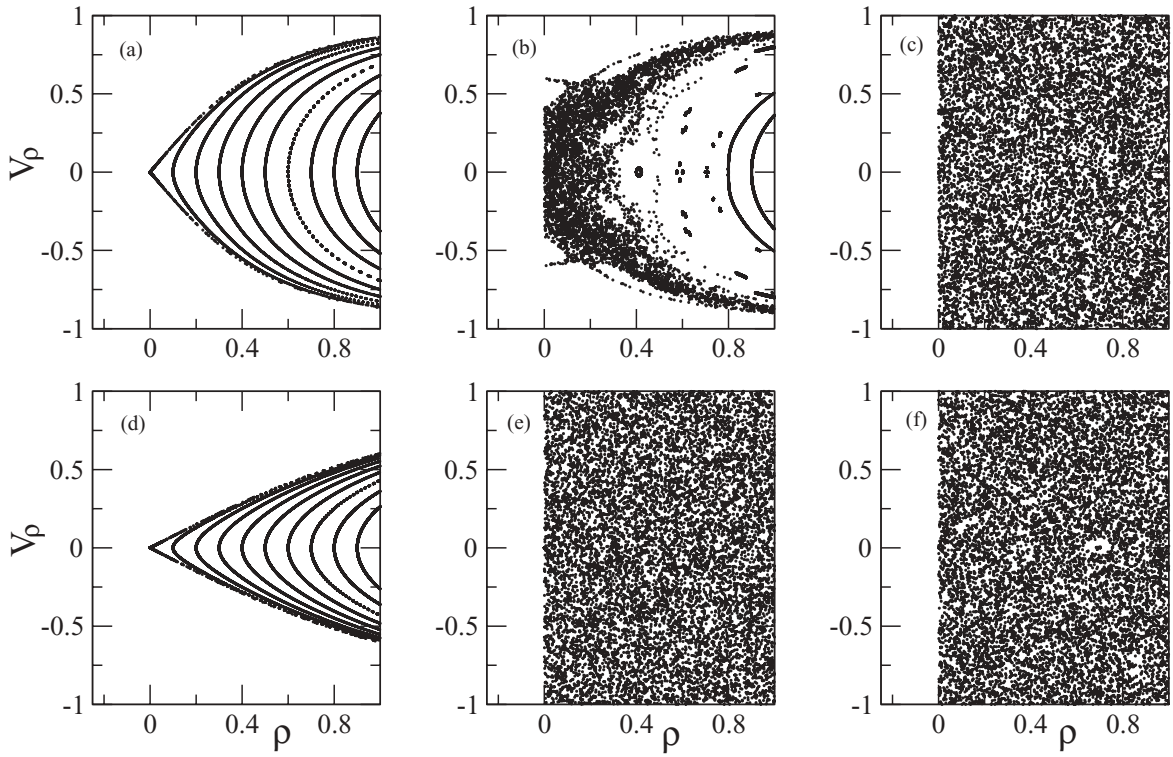

FIG. 7. Poincaré sections v_ρ vs ρ for spheroid [(a) and (d)], P_2 [(b) and (e)] and P_5 [(c) and (f)] shapes at the small deformation $\alpha = 0.1$ [(a)–(c)] and large deformation $\alpha = 0.4$ [(d)–(f)] for the projections of the angular momentum on the symmetry axis $m = 0$.

a more pronounced Wigner-like distribution with increasing multipolarity n and deformation α in Fig. 6, especially remarkable at P_5 surface distortions and sufficiently large deformation $\alpha = 0.4$ [see last plot (d) in Fig. 6]. Including all the angular momentum projections m for all desired multipolarities and deformations one has clearly Poisson-like behavior, although they differ essentially in numbers $\mathcal{A}$, $\mathcal{B}$ from the standard ones (1,0) (see Fig. 5). The reason for this effect is mainly associated with the same loss of the symmetry degree $\mathcal{K}$ from the partially integrable 3D motion ($\mathcal{K} = 1$) for full-spectrum calculations to the chaotic nonintegrable 2D one ($\mathcal{K} = 0$) with the fixed m. Note also that we choose the magnitude of the spacing ΔS for our chaoticity parameter (see Appendix) which would ensure a *smooth* NNSD. Therefore, we expect smaller influence of the degeneracies due to crossings of the SP levels with different values of m (see Figs. 1 and 2) on the NNSD. This is similar to the *smooth* level density $\tilde{g}$ which can be well approximated by the extended Thomas-Fermi approach ignoring such degeneracies.

In addition, one can study the chaoticity properties of the $m = 0$ spectra depending on the deformation and multipolarities by looking at the Poincaré sections shown in Fig. 7 [10,14,18]. The upper row is related to a small deformation and the lower row corresponds to a large deformation. The projection of the angular momentum is $m = 0$ in all pictures of Fig. 7. The difference is remarkable for the integrable spheroidal cavity and other nonintegrable (in the plane of the symmetry axis) shapes. As seen by comparing upper and lower plot lines, with increasing deformation α and multipolarity n, we find more chaotic behavior and we should expect therefore the NNSD to be closer to the Wigner distribution (9). This is in agreement with the NNSD calculations for the fixed $m = 0$ (see Fig. 6), especially for larger deformation ($\alpha = 0.4$) and multipolarity ($n = 5$). Notice that similar properties of the NNSD for other potentials and constraints were discussed in Refs. [23–26].

The difference between the NNSD calculations with the realistic level densities by the Strutinsky shell-correction method [see Eq. (4)] for the considered WS potential and those with their idealistic linear behavior [Eq. (10)] can be studied in terms of the general formula $P(S)$ [Eq. (5)]. In particular, the shell effects related to the inhomogeneity of the SP levels near the Fermi surface for all desired multipolarities and deformations are found to be significant, also in relation to the fixed quantum number m.

Figures 8 and 9 show the results of these calculations corresponding to Figs. 5 and 6. Notice that, in the case of the full spectra (see Fig. 8), one has Poisson-like distributions corresponding to the smooth density (dashed) with a similar behavior as NNSD shown by heavy dots, in contrast to Fig. 9 where we find rather big differences between these curves. The shell effects are measured by the differences between the solid curve related to the total level density with the shell components and the dashed curve for the smooth level density of Figs. 3 (all m) and 4 (with $m = 0$) (see Figs. 8 and 9, respectively). In contrast to the NNSD corresponding to

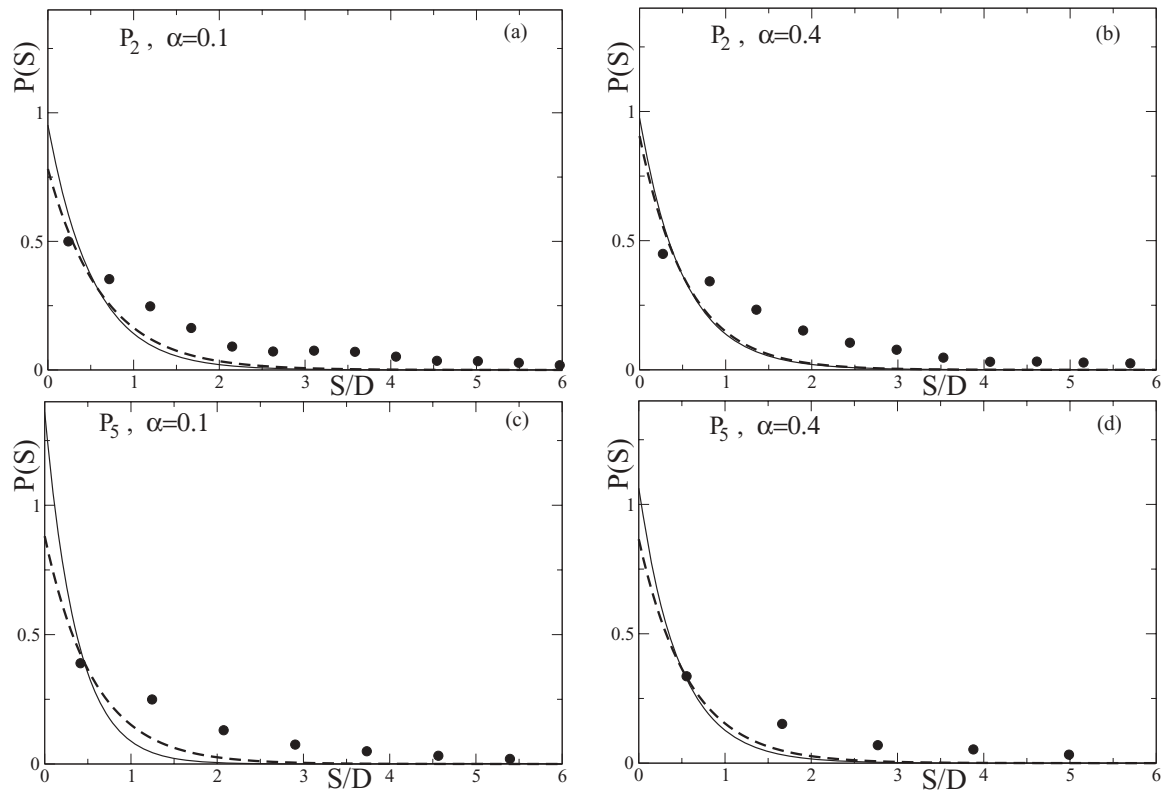

FIG. 8. General distribution $P(S)$ [Eq. (5)] vs energies S for same spectra as in Figs. 1, 3, and 5; dashed lines are the distributions $P(S)$ related to the Strutinsky smooth density $\tilde{g}(S)$ and solid line is the total level density $g_\Gamma(S)$ [Eq. (4)]; dots are the same as in Figs. 5 and 6.

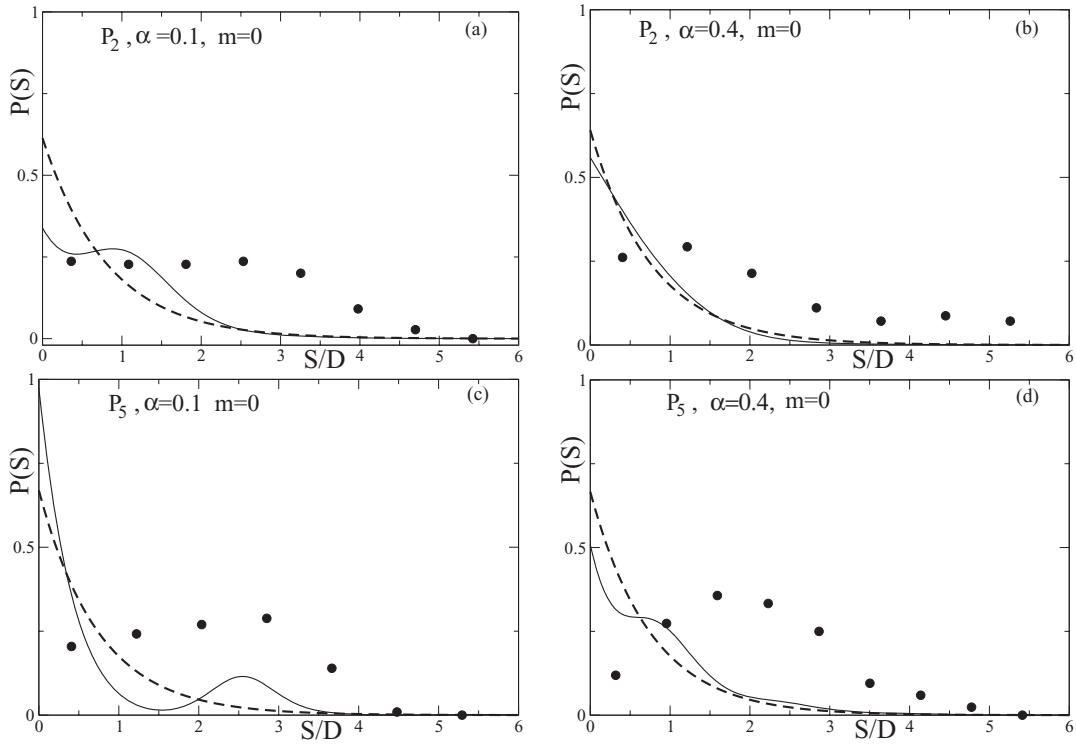

FIG. 9. Same as in Fig. 8 but for spectra of Figs. 2, 4 and 6.

the smooth component $\tilde{g}$ of the level density [see Eq. (4)], its fluctuating shell correction δg depends essentially on the degeneracies related in particular to the level crossings mentioned above in connection with Figs. 1 and 2 and level density calculations (see Figs. 3 and 4). This is one of the possible important reasons for spurious effects of the integrability in the NNSD which might explain to some extent the differences between the solid curves and heavy dots for the NNSD in Fig. 9, see also such smaller differences in Fig. 8, too. Note also that, with increasing deformations, one has slightly decreasing shell effects, in contrast to the multipolarity dependence for which there is almost no change in the shell effects at the same deformations.

V. CONCLUSIONS

We studied the statistics of the neighboring SP levels in the WS potential for several typical multipolarities and deformations of the surface shapes and deformations, as compared with the standard Poisson and Wigner distributions $P(S)$. For the sake of comparison, we derived analytically the combine asymptotic Poisson-Wigner distribution $P(S)$ related to the general linear dependence of the corresponding single-particle level density. We found significant differences between distributions for a fixed value of the angular momentum projection m of the particle and those accounting for all possible values of m. For the case of the fixed $m = 0$ we obtained distributions $P(S)$ more close to the Wigner shape with the maximum between $S = 0$ and a maximal large value of S, the more pronounced the larger multipolarity and deformation of the potential surface. We also found that the full spectra distributions $P(S)$ look Poisson like in a sense that they have maximum at $S = 0$ and an almost-exponential decrease as a function of energy near the Fermi surface. Our results clarify the widely extended opinion of the relation of the distributions (Poisson or Wigner) to the integrability of the problem (the integrable or chaotic one). All considered potentials are axially symmetric but they are the same *nonintegrable* ones in the plane of the symmetry axis. The degree of symmetry which determines the classical degeneracy [22,27,28] $\mathcal{K}$ (see introduction) for the case of the full spectra (Figs. 1, 3, 5) is higher than for the fixed angular momentum m ($\mathcal{K} = 0$). This is the effect of decreasing the phase-space volume (accessible for the particle motion) from a partially integrable 3D system with $\mathcal{K} = 1$ to the completely chaotic nonintegrable 2D-like system ($\mathcal{K} = 0$). Notice that integrability is not only one criterion of the absence of chaoticity. The measure of the differences of the distributions $P(S)$ between Poisson and Wigner standard distributions depends also on the properties of the energy dependence of the level density (from constant to proportional-to-energy dependence). From comparison between the general distribution $P(S)$ related to the smooth level density obtained by the Strutinsky shell correction method and the statistics of the neighboring SP levels, one finds that all of them are more close to the Poisson-like behavior. This shows that the energy dependence of the smooth level density differs much from the linear functions. We obtained also large shell effects in the distributions $P(S)$, in nice agreement with those in the key quantity in this analysis—level density dependencies at an energy near the Fermi surface. We should point out also a possible spurious effect of the integrability on the NNSD

due to the degeneracies related to crossings of the SP levels if the shell corrections to the level density are included in these calculations.

Regarding perspectives, it might be necessary to use the combined microscopic-macroscopic approaches [6,7] and semiclassical POT [29] to clear up the results more systematically and analytically. Our quantum results can be interesting for understanding the one-body dissipation at slow and faster collective dynamics with different shapes like the ones met in nuclear fission and heavy-ion collisions.

ACKNOWLEDGMENTS

We thank S. Åberg, V. A. Plujko, and S. V. Radionov for valuable discussions.

APPENDIX: A DERIVATION OF NNSD

In our derivations of the NNSD $P(S)$ we follow basically Refs. [1,3,5] in order to better clarify the role of the given SP level density $g(S)$ of the spacing argument S which specifies the function $f(x)$ of the spacing variable x in notations of Ref. [1], $r_{10}(S)$ in Ref. [3], or $r(x)$ $(x \equiv S)$ in Ref. [5]. We introduce first the level density,$g(E)$ as the number of levels dN in the energy interval $[E, E + dE]$ divided by the energy interval $g(E) = dN/dE$. With the help of this quantity one can derive the NNSD $P(S)$ as the probability density versus the spacing S between the nearest-neighboring levels. Specifying thus $P(S)$ to the problem with the known SP spectra of the Hamiltonian, one can split the energy interval ΔE under investigation into many small (equivalent for simplicity) parts $\Delta S \ll \Delta E$. Each of ΔS nevertheless contains many energy levels; $\Delta S \gg D$. Then, we find the number of the levels which occur inside of a small interval ΔS. Normalizing these numbers by the total number of the levels inside the total energy interval ΔE one obtains the distribution which we shall call the probability density $P(S)$. Notice that the result of this calculation depends on the energy length of the selected ΔS which plays here a role of the chaotic element of the introduced ensemble. In our calculations, we select ΔS by the condition of a sufficient smoothness of the distribution $P(S)$. Such a procedure is often used for the statistical treatment of the experimentally obtained spectrum with fixed quantum numbers, like angular momentum, parity, and so on [3].

Following now mainly Ref. [5], let us calculate first the intermediate quantity $f(S)$ as the probability that there is no energy level in the energy interval $[E, E + S]$. According to the general definition of the level density mentioned above, $g(S)dS$ can be considered as the probability that there is one energy level in $[E + S, E + S + dS]$. Then,

$$f(S + dS) = f(S)[1 - g(S)dS], \tag{A1}$$

which leads to the differential equation for $f(S)$,

$$df = -g(S)dSf(S). \tag{A2}$$

Solving this equation one gets

$$f(S) = C \exp\left(- \int_0^S g(x)dx \right). \tag{A3}$$

Let $P(S)dS$ denote the probability that the next energy level is in $[E + S, E + S + dS]$,

$$P(S)dS = f(S)g(S)dS. \tag{A4}$$

Then, substituting Eq. (A3) into Eq. (A4) one finally arrives at the general distribution:

$$P(S) = Cg(S) \exp\left(- \int_0^S g(S')dS' \right). \tag{A5}$$

The boundary conditions in solving the differential equation (A2) accounts for the meaning of the NNSD $P(S)$ and its argument as the spacing between the nearest-neighbor levels as shown in the integration limit in Eq. (A5). The constant C is determined from the normalization conditions [Eq. (6)].

[1] C. E. Porter, *Statistical Theories of Spectra: Fluctuations* (Academy Press, New York, 1965).

[2] E. P. Wigner, Proc. Cambridge Philos. Soc. **47**, 790 (1951); *Canadian Math. Congress Proceedings* (University of Toronto Press, Toronto, 1957), p. 174; SIAM Rev. **9**, 1 (1967).

[3] T. A. Brody *et al.*, Rev. Mod. **53**, 385 (1981).

[4] M. L. Mehta, *Random Matrices* (Academic Press, San Diego, New York, Boston, London, Sydney, Tokyo, Toronto 1991).

[5] S. Åberg, *Quantum Chaos* (Mathematical Physics, Lund, 2002).

[6] W. D. Myers and W. J. Swiatecki, Nucl. Phys. **81**, 1 (1966) ; Ann. Phys. (NY) **55**, 395 (1969).

[7] V. M. Strutinsky, Nucl. Phys. A **95**, 420 (1967); **122**, 1 (1968).

[8] J. Blocki, Y. Boneh, J. R. Nix, J. Randrup, M. Robel, A. J. Sierk, and W. J. Swiatecki, Ann. Phys. (NY) **113**, 330 (1978).

[9] J. Blocki, J. Skalski, and W. J. Swiatecki, Nucl. Phys. B **594**, 137 (1995).

[10] J. Blocki, J.-J. Shi, and W. J. Swiatecki, Nucl. Phys. A **554**, 387 (1993).

[11] J. Blocki, J. Skalski, and W. J. Swiatecki, Nucl. Phys. A **618**, 1 (1997).

[12] C. Jarzynski and W. J. Swiatecki, Nucl. Phys. A **552**, 1 (1993).

[13] P. Magierski, J. Skalski, and J. Blocki, Phys. Rev. C **56**, 1011 (1997).

[14] J. P. Blocki, A. G. Magner, and I. S. Yatsyshyn, At. Nucl. Energy **11**, 239 (2010); Int. J. Mod. Phys. E **20**, 292 (2011).

[15] S. E. Koonin and J. Randrup, Nucl. Phys. A **289**, 475 (1977).

[16] A. G. Magner, A. M. Gzhebinsky, and S. N. Fedotkin, Phys. Atom. Nucl. **70**, 647 (2007); **70**, 1859 (2007).

[17] A. M. Gzhebinsky, A. G. Magner, and S. N. Fedotkin, Phys. Rev. C **76**, 064315 (2007).

[18] R. Arvieu, F. Brut, J. Carbonell, and J. Touchard, Phys. Rev. A **35**, 2389 (1987); Nucl. Phys. A **545**, C497 (1992).

[19] W. D. Heiss, R. G. Nazmitdinov, and S. Radu, Phys. Rev. Lett. **72**, 2351 (1994).

[20] W. D. Heiss and R. G. Nazmitdinov, Phys. Rev. Lett. **73**, 1235 (1994).

[21] M. Brack *et al.*, Rev. Mod. Phys. **44**, 320 (1972).

[22] A. G. Magner, I. S. Yatsyshyn, K. Arita, and M. Brack, Phys. At. Nucl. **74**, 1475 (2011).
[23] W. D. Heiss, R. G. Nazmitdinov, and S. Radu, Phys. Rev. C **52**, 3032 (1995).
[24] W. D. Heiss and R. G. Nazmitdinov, Physica D **118**, 134 (1998).
[25] A. Hamoudi, R. G. Nazmitdinov, E. Shahaliev, and Y. Alhassid, Phys. Rev. C **65**, 064311 (2002).
[26] R. G. Nazmitdinov, E. I. Shahaliev, M. K. Suleymanov, and S. Tomsovic, Phys. Rev. C **79**, 054905 (2009).
[27] V. M. Strutinsky and A. G. Magner, Sov. J. Part. Nucl. **7**, 138 (1976).
[28] V. M. Strutinsky, A. G. Magner, S. R. Ofengenden, and T. Døssing, Z. Phys. A **283**, 269 (1977).
[29] M. Brack and R. K. Bhaduri, *Semiclassical Physics*. *Frontiers in Physics* (Addison-Wesley, Reading, 1997), Vol. 96, 2nd ed. (Westview Press, Boulder, 2003).
[30] M. C. Gutzwiller, J. Math. Phys. **12**, 343 (1971); M. C. Gutzwiller, *Chaos in Classical and Quantum Mechanics* (Springer-Verlag, New York, 1990).
[31] M. V. Berry and M. Robnik, J. Phys. A **17**, 2413 (1984).
[32] A. Y. Abul-Magd and M. H. Simbel, Phys. Rev. C **54**, 1675 (1996).